HHS Public Access

Author manuscript

Nat Struct Mol Biol. Author manuscript; available in PMC 2017 January 06.

Published in final edited form as:

Nat Struct Mol Biol. 2016 March ; 23(3): 256–263. doi:10.1038/nsmb.3166.

The bacterial dicarboxylate transporter, VcINDY, uses a two-domain elevator-type mechanism

Christopher Mulligan[1], **Cristina Fenollar-Ferrer**[2,3], **Gabriel A. Fitzgerald**[1], **Ariela Vergara-Jaque**[2], **Desirée Kaufmann**[3,5], **Yan Li**[4], **Lucy R. Forrest**[2,3], and **Joseph A. Mindell**[1]

[1]Membrane Transport Biophysics Section, National Institute of Neurological Disorders and Stroke, National Institutes of Health, Bethesda, MD 20892

[2]Computational Structural Biology Unit, National Institute of Neurological Disorders and Stroke, National Institutes of Health, Bethesda, MD 20892

[3]Protein/Peptide Sequencing Facility, Porter Neuroscience Research Center, National Institute of Neurological Disorders and Stroke, National Institutes of Health, Bethesda, MD 20892. [3]Max Planck Institute of Biophysics, Frankfurt am Main, Germany

[4]Protein/Peptide Sequencing Facility, Porter Neuroscience Research Center, National Institute of Neurological Disorders and Stroke, National Institutes of Health, Bethesda, MD 20892

Abstract

Secondary transporters use alternating access mechanisms to couple uphill substrate movement to downhill ion flux. Most known transporters utilize a “rocking bundle” motion, where the protein moves around an immobile substrate binding site. However, the glutamate transporter homolog, Glt_{Ph}, translocates its substrate binding site vertically across the membrane, an “elevator” mechanism. Here, we used the “repeat swap” approach to computationally predict the outward-facing state of the Na^+/succinate transporter VcINDY, from *Vibrio cholerae*. Our model predicts a substantial “elevator”-like movement of vcINDY’s substrate binding site, with a vertical translation of ~15 Å and a rotation of ~43°; multiple disulfide crosslinks which completely inhibit transport provide experimental confirmation and demonstrate that such movement is essential. In contrast, crosslinks across the VcINDY dimer interface preserve transport, revealing an absence of large scale coupling between protomers.

To whom correspondence should be addressed: Lucy R. Forrest (lucy.forrest@nih.gov) and Joseph A. Mindell (mindellj@ninds.nih.gov).

[5]Present address: Institute of Molecular Biology, Mainz, Germany.

Accession Codes:

The model has been submitted to the Protein Model Database (https://bioinformatics.cineca.it/PMDB/) with identifier PM0080216.

Author Contributions: LRF and JAM conceived the project, CFF, AVJ and DK carried out computational modeling; CFF and LRF analyzed data and directed computational modeling efforts. JAM and CM designed and planned experiments. CM performed experiments, and supervised GF, who performed dimer interface experiments. YL performed Mass Spectroscopy and Interpreted MS data. CM, CFF, LRF, and JAM wrote the manuscript.

Introduction

Secondary active transporters constitute a large class of proteins responsible for catalyzing the passage of key compounds across the lipid bilayer in all living cells. These molecular machines harness the energy supplied by the electrochemical gradient of one solute, usually a coupling ion like H^+ or Na^+, to power the transport of another solute against its concentration gradient. Secondary transporters operate by an alternating access mechanism in which conformational changes in the protein alternately expose the substrate-binding site to either side of the membrane. A minimum of two conformational states are therefore required to achieve alternating access; an inward-facing state, where the substrate is accessible to the cytoplasmic side of the membrane only, and an outward-facing state, where the substrate is only accessible to the extracellular side[1,2]. Many transporters also utilize intermediate “occluded” states in which the substrate-binding site is accessible to neither side of the membrane[3–5].

The ever-growing collection of secondary transporter crystal structures reveals a remarkable diversity of protein folds; structural and functional investigations have begun to illuminate the conformational mechanisms by which these folds achieve alternating access. Of the 17 secondary transporter folds reported to date, the Major Facilitator Superfamily (MFS) fold and the LeuT fold represent a majority of the known protein sequences and an overwhelming majority of the known X-ray crystal structures[6,7]. In both cases, their conformational mechanisms involve movement of helices around a substrate binding site, which is usually situated at the center of the lipid bilayer. While the overall mechanism has been described as movements of domains in “rocking bundle” or “rocker-switch” type conformational changes, the available evidence also suggests a role for individual “gating” helices that help determine intermediate steps in the transport cycle[8–12]. Either way, for both of these large families, the substrate retains its relative position in the membrane regardless of the conformation of the transporter.

A dramatically different route to achieving alternating access involves an elevator-type (or “carrier”) mechanism; here, the substrate-binding site itself is moved. Elevator-type transporters are composed of two domains; a scaffold domain that remains relatively rigid during the transport cycle, and a second domain that contains all the residues necessary to bind the substrate, referred to as the transport domain. This mechanism derives its name from the elevator-like rigid body translation of the transport domain back and forth across the hydrophobic barrier provided by the protein and lipid bilayer, which is achieved by moving the entirety of the substrate-binding site, thereby allowing the substrate to be alternately exposed to both sides of the membrane. To date, only the glutamate transporter homolog GltPh has been convincingly shown to employ an elevator-like mechanism[13,14]. GltPh belongs to a relatively small family of proteins (the dicarboxylate/amino acid:cation symporters, DAACS; transporter classification database (TCDB) family 2.A.23), raising the possibility that its mechanism is unique to this small family. However, a similar mechanism has recently been hypothesized for the Na^+/H^+ antiporters, though this proposal remains controversial[15]. Thus, the prevalence of elevator-like mechanisms in biology remains a compelling and unanswered puzzle.

Here, using structural modeling combined with extensive disulfide crosslinking, biochemical, and functional characterization of purified VcINDY, we report that the Na^+/succinate transporter VcINDY also employs an elevator-type mechanism. VcINDY, from *Vibrio cholerae*, belongs to the divalent anion sodium symporter (DASS) family of transporters (TDCB family 2.A.47), which also contains members of the SLC13 family responsible for the uptake of citrate, Krebs cycle intermediates, and sulfate, in humans[16–18]. VcINDY is the only DASS family member for which a high-resolution structure is known[19]. The 3.2 Å structure of VcINDY reveals a dimeric architecture; the positioning of the bound ligand, in this case citrate, indicates that this structure reflects an inward-facing state of this transporter. Each protomer consists of 11 transmembrane (TM) helices that can be partitioned into two distinct domains; a scaffold domain that forms all inter-protomer contacts and a transport domain that houses the substrate binding site (Fig. 1 and 2) – an arrangement highly reminiscent of Glt_{Ph}.

The results presented here computationally predict and experimentally confirm an outward-facing state of VcINDY, and indicate that a ~15 Å translation accompanied by a ~43° rigid body rotation of the transport domain occurs to expose the substrate binding site to the external solution. This work therefore reveals a second transporter family, with a different fold than Glt_{Ph}, that employs an elevator- type mechanism with similarities to that of Glt_{Ph}, but also with key differences. Given the relationship between VcINDY and other families in the large "Ion Transporter (IT) Superfamily" we raise the possibility that this superfamily shares key features of the elevator mechanism and that, like the rocking bundle- type mechanisms, this conformational strategy is also widespread in secondary transport[20–22].

Results

VcINDY contains inverted-topology structural repeats

For VcINDY, only the inhibitor-bound, inward-facing state structure is available[19]. We sought to explore additional conformations of VcINDY using repeat-swap homology modeling, wherein we identify repeating structural units in the crystal structure, then swap the conformations of these repeating units[23]. Underlying the success of this procedure in previous studies is the fact that the structures of the repeating units are not perfectly symmetric; any subtle conformational differences between the repeating units can lead to the prediction of alternate conformational states[13,23–26].

VcINDY contains an inverted-topology structural repeat related by pseudo two-fold symmetry around an axis in the plane of the membrane[19]; repeat unit 1 (RU1) consisting of TM helices 2–6 (defined here as residues 42–242) and repeat unit 2 (RU2) consisting of TM helices 7–11 (residues 260–453; Fig. 1a, Fig 1b). TM1 is a peripheral helix in VcINDY and is not part of either repeating unit. Our alignments of the amino acid sequences of RU1 and RU2 revealed a low sequence identity of ~20% (Supplementary Fig. 1a). However, upon superimposition of the repeating units, we clearly see that they share a similar architecture, with a root mean square deviation (RMSD) value for the Cα atoms of ~4.3 Å (Fig. 1c). When we compared only the transport domain or scaffold domain we found much higher structural similarity (RMSD values of 2.0–2.1 Å) suggesting that the main contribution to

the structural differences between the repeats comes from the orientation of the transport domain helices relative to the scaffold domain helices (Fig. 1c).

Predicting an outward-facing state of VcINDY

We applied the repeat-swap procedure to VcINDY by modeling the conformation of RU1 using RU2 as a template, and vice versa (Fig. 1 and Fig. 2a, Supplementary Fig. 1b). The resulting model reveals a substantial conformational change compared to the inward-facing crystal structure (Fig. 2b). As a result of this conformational change, which involves movements of transport domain relative to the scaffold domain, the substrate binding site becomes exposed to the extracellular side of the membrane; thus the repeat-swapped model clearly represents a putative outward-facing state of VcINDY (Fig. 2c and Supplementary Fig. 2a and b).

To analyze the conformational changes that occur during the transformation from the inward- to the outward-facing conformation, we superimposed the model onto the structure using only helices from the oligomerization interface, which also allowed us to construct a model of the dimer (Fig. 2b). We note that this dimer model is therefore based on the assumption that the dimer interface is unchanged during transport (tested explicitly below). Comparison of the two states predicts that the entire transport domain undergoes a ~15 Å vertical translation accompanied by a ~43° rotation as it transitions from inward-to outward-facing states (Supplementary Fig. 2, Supplementary Movie 1).

Design of cysteine pairs to test the outward-facing model

The outward-facing model suggests that transport requires a major translocation of the transport domain, accompanied by a significant rotation. If such a motion indeed occurs, then there should be residues that are far apart in one state, but that are brought into close proximity in the other state. We tested this idea by introducing pairs of cysteine residues at positions that are widely separated in the inward-facing structure (Cβ-Cβ distance >12 Å), but are brought closely enough together (Cβ-Cβ distance <7 Å) in the predicted outward-facing state that they could potentially form disulfide links. We predict that crosslinking these residue pairs should confine the protein to a single state in the transport cycle, thereby strongly inhibiting transport. To validate this approach, we also designed a cysteine pair that should selectively stabilize the known inward-facing state by substituting residues that are distant in the outward-facing model, but in close proximity in the inward-facing crystal structure.

As a starting construct, we used a mutant in which the three native cysteines were replaced with serine. This protein catalyzes effectively catalyzes Na^+-driven succinate uptake (Supplementary Fig. 3a). From 18 candidate pairs, we selected three double mutants for further examination: T154C V272C, A120C V165C, and A436C V364C (see Methods for distances). Together, these cysteine pairs occupy three different positions at the interface between the transport and scaffold domains, providing good coverage of the conformational change predicted by our model. To stabilize the inward-facing state, we introduced the double cysteine mutant L60C S381C (Supplementary Fig. 4a). All four cysteine pairs were

well tolerated by VcINDY (Supplementary Fig. 3b) and demonstrated robust transport activity (see below).

Cysteine crosslinking supports the outward-facing model

We screened for successful crosslinks using the gel-shift assay described by Basilio et al[27], using either $HgCl_2$, which can act as a homobifunctional crosslinking reagent, or the oxidizing agent copper phenanthroline (CuPhen), to catalyze disulfide bond formation. Specifically, after treatment with crosslinker, we enumerated the remaining free cysteines by treating the protein with 5 kDa PEG-maleimide (mPEG5K), which causes a substantial shift in the protein's gel mobility upon reaction with free cysteine. If the introduced cysteines are crosslinked with each other, however, then they will be unable to react with mPEG5K and the protein band will run as monomeric VcINDY on SDS-PAGE. Before crosslinking, each double cysteine mutant was almost completely PEGylated after incubation with mPEG5K, demonstrating that both cysteines were accessible to the probe (Fig. 3 and Supplementary Fig. 4b). In contrast, after treatment with crosslinker all three outward-stabilizing double cysteine mutants (Fig. 3, Supplementary Fig. 5) and the inward-stabilizing mutant (Supplementary Fig. 4b) were completely protected from PEGylation, suggesting that all four double mutants successfully formed intramolecular crosslinks. Treatment of the double cysteine mutants with crosslinking reagents did not significantly affect the elution volume of the protein peak on Size Exclusion Chromatography (SEC), but did result in slight peak broadening; we observed minimal aggregation for these proteins (data not shown). Treating the six single cysteine mutants with either Hg^{2+} or CuPhen revealed proteins running primarily as monomers on SDS PAGE (Supplementary Fig. 6). Several single cysteine mutants, e.g. V364C and V165C, showed some dimerization in the presence of $HgCl_2$; however, the lack of dimerization observed in double mutants containing these same mutations further supports the conclusion that intramolecular disulfides are forming between the introduced cysteines and not between protomers. These results indicate that treatment with crosslinking reagent is well tolerated and that the fold of the crosslinked protein is intact.

To obtain direct physical evidence of crosslink formation we analyzed the double cysteine mutants using liquid chromatography-tandem mass spectrometry (LC-MS/MS, Fig. 4). If we indeed formed crosslinks in the cysteine mutants then we should be able to directly detect the crosslinked peptides using this approach. After incubating the cysteine mutants with either CuPhen or dithiothreitol (DTT; to prevent spontaneous crosslink formation) we digested the proteins, and acquired Mass Spectrometry (MS) and MS/MS spectra of the resulting peptides. We identified the expected disulfide-crosslinked peptides in the CuPhen-treated samples of both A120C V165C and T154C V272C (Fig. 4); these peptides were completely absent in the reduced protein samples (Fig. 4a and b, right panel). We also detected a peptide consistent with crosslink formation between A346C and V364C. However, the size of the peptide and the quality of the MS/MS spectrum prevented us from confidently assigning the MS fragment peaks (data not shown). Due to the same technical limitation, we were also unable to obtain consistent LC-MS/MS data for the inward-stabilizing mutant L60C S381C. As a negative control for crosslink formation, we performed MS on the A120C V364C mutant, in which the cysteines should never be close

enough to form a disulfide bond. For this protein, we observed no evidence of crosslink formation in the MS experiments, nor was the 120C-containing peptide depleted from the spectra, confirming that these cysteines (distant in either structure) do not react with each other (again the 364C peptide is difficult to observe for technical reasons). These data unequivocally demonstrate crosslink formation between two of the introduced cysteine pairs, and strongly suggest that the mPEG5K labeling results for the other two pairs indeed reflect crosslink formation. Formation of these crosslinks strongly supports our prediction that the outward facing conformation of VcINDY requires a specific, large excursion of the transport domain (Supplementary Movie 2).

Crosslinking VcINDY abolishes transport activity

Our hypothesis for the VcINDY transport mechanism, based on the model of the outward-facing conformation, is that the translocation of the transport domain is essential for transport, physically moving the binding site from one side of the membrane to the other (Fig. 2 and Supplementary Movie 1). If true, then crosslinking VcINDY in either the inward- or outward-facing state should straightjacket the transporter and curtail its transport activity. We tested this prediction by reconstituting the double cysteine mutants into proteoliposomes and measuring succinate transport activity in the presence and absence of a disulfide link (Fig. 5). Indeed, when we form crosslinks by treating proteoliposomes containing double cysteine mutants with excess $HgCl_2$ (on both sides of the membrane) we observed almost complete cessation of succinate transport activity for all three outward-stabilizing cysteine mutants (Fig. 5) and for the inward-stabilizing mutant (Supplementary Figure 4c). Transport activity was almost completely restored (except for T154C V272C, which regained ~60% of its transport activity) when the crosslinks were reduced, indicating that the abolition of transport was caused by disulfide bond formation. The retention of substantial transport activity in the $HgCl_2$-treated Cysless protein confirms that the strong inhibition in the crosslinked proteins is due to the specific effects of the crosslinking agents on the double cysteine mutants. Together these results strongly support our hypothesis that the large conformational change required to form the crosslinks is also an essential component of the transport process.

Rigidity of the dimer interface during transport

The data described so far demonstrate large-scale conformational changes between helices in the scaffold and helices in the transport domain. In constructing a model of the outward-facing dimer, as described above, we made the assumption that the helices contributing to the oligomerization interface (i.e., from the scaffold), remain fixed relative to one another. We tested this assumption by assessing the functional effects of “stapling” the protomers together at several inter-protomer contact points[28]. If substantial conformational changes at the dimer interface are essential for transport then stapling the protein at these positions should abolish transport activity.

We introduced cysteine pairs into the dimer interface at 4 contact points (Fig. 6a); Q86C (helix 4a) and S95C (TM4b); V68C (TM3) and S304C (TM8); N90C (helix 4a); and K316C (TM9). Due to the two-fold symmetry of the VcINDY homodimer, we expected the mutants containing two cysteine residues per protomer to form two disulfide bonds across the

interface, whereas we expected the corresponding single cysteine mutants to form single disulfide bonds (with their symmetry-related counterparts in the other protomer). Each interfacial cysteine mutant was stable and exhibited transport activity when reconstituted into liposomes (Fig. 6 and Supplementary Fig. 7).

Inter-protomer crosslinks formed readily upon incubation with CuPhen, as reflected by a shift of the protein band from the monomeric VcINDY molecular weight to that expected for the dimer on SDS PAGE, and remain stable upon reconstitution into proteoliposomes (Fig. 6b). Incubation with 10 μM 2:1 CuPhen for 45 minutes at room temperature fully crosslinked all proteins except for the V68C S304C mutant: V68C/S304C required 500 μM CuPhen to attain full crosslinking, which presumably reflects reduced accessibility of these residues to the crosslinking agent or sub-optimal alignment of the two cysteines.

All four “stapled” mutants still transport succinate after crosslink formation (Fig. 6c), demonstrating that there are no substantial conformational changes in these positions that are essential for transport (Fig. 6c). However, the functional effects of stapling the dimer interface varied depending on the position of the disulfide crosslink. Crosslinking two of the mutants, V68C S304C and N90C, had no discernable effect on their transport activity beyond the non-specific effects we observed for Cysless (Fig. 6c, see Methods for discussion of the effects of reducing agents on activity). Interestingly, however, crosslinking the other two mutants, Q86C S95C and K316C, resulted in 5-fold and 2-fold transport activity decreases, respectively. A possible explanation is that the crosslinking causes a local distortion in the scaffold domain that reduces the ability of the transport domain to move along it, or that transport is facilitated by some movement within the dimer interface that is impeded by the crosslink. Further experiments will be necessary to illuminate the underlying causes of these more subtle effects.

Discussion

In this study, we present a structural model of the outward-facing state of VcINDY along with extensive supporting experimental data. This work demonstrates that VcINDY utilizes an elevator-type movement, with protein excursions on the order of ~15 Å, that is an essential step in the transport cycle. Formation of disulfide crosslinks in three different locations, each physically separated in the inward-facing structure but predicted by our model to be juxtaposed in the outward-facing state, shows that the protein can adopt the predicted outward-facing conformation. That the crosslinks profoundly disrupt transport confirms that movement to and from this state is essential for transport. In contrast, preservation of transport activity in the presence of crosslinks across the dimer interface reveals that no major conformational change in this region is required for activity.

As repeat-swap modeling is, in essence, a homology modeling technique, the error of the model depends on the difference in the sequences of the two repeats; in the case of VcINDY the two repeats contain ~20% identical residues, implying a structural error of 1–3 Å in the Cα positions[26,29,30]. However, our updated protocol reduces this error significantly, by including a second refinement step that effectively maintains the integrity of the domains moving relative to one another, while preserving the overall movement of those domains

(see Methods; Supplementary Figs. 2 and 9). Our results suggest that the transport domain moves vertically ~15 Å and rotates ~43°, thereby translocating the substrate binding site to the other side of the hydrophobic barrier provided by TM helices 4 and 9 (Figure 7). Insofar as the X-ray structure represents an actual inward facing state of VcINDY, we expect our model to accurately represent the outward facing state. However, as discussed previously[26], if the structure does not represent the true inward facing state, we expect our model to deviate accordingly. The success of our experimental test of the model, with multiple crosslinks capturing the outward-facing state, strongly suggests that the modeled conformation represents a native state, with errors of a few Å, and that the conformational change is truly elevator-like.

A key assumption underlying our results is that the states stabilized by our crosslinks represent well-populated conformations accessible to the native protein rather than rarely-visited grotesques that have been kinetically trapped by the disulfide bond. We report crosslinks between three different cysteine pairs, distributed across the transport/scaffold domain interface. This combination of appositions would be extraordinarily difficult to achieve with a fundamentally different conformational change. Moreover, the wide range of conditions used in these experiments, including crosslink formation using either CuPhen or $HgCl_2$ with protein in either detergent or lipid membranes, argues that we are sampling a native state of the protein. In addition, the consistent mobility of the crosslinked protein on size exclusion chromatography rules out the possibility of a reversibly denatured form of the protein that is stabilized by the crosslink. How does the movement of VcINDY compare with other proposed elevator-type transporters? Currently, the only transporter that can indisputably be called an elevator-type transporter is the glutamate transporter homolog, Glt_{Ph} [14,31]. Our results demonstrate that the transport domain of VcINDY undergoes a similar perpendicular and rotational movement to that of Glt_{Ph} (~15 Å and 43° for VcINDY vs. 16 Å and 37° for Glt_{Ph})[14].

Recently, it has been suggested that members of the cation-proton antiporter (CPA) family, exemplified by the Na^+/H^+ exchanger NhaA, employ an elevator-type mechanism, although this remains controversial. Several lines of evidence, both theoretical and experimental, suggest that in *E. coli* NhaA a panel of four TM helices rotate within the plane of the membrane in order to open and close the inward and outward-facing pathways[25], a “rocking bundle” However, a recent structural comparison of NhaA and NapA, a remote homolog, was interpreted as consistent with an elevator-type movement[15]. However, NapA shares <15% identical residues with NhaA, casting doubt on any conclusions based on this direct comparison. Furthermore, more recent structural analysis of two other CPA family members, PaNhaP and MjNhaP1, suggest that only slight conformational changes are required for transport[32,33]. The structure of a bacterial concentrative nucleoside transporter, VcCNT, also reveals the hallmarks of an elevator-type transporter, although its structure has so far only been captured in an inward-facing state[34,35]. Interestingly, repeat-swap modeling of VcCNT predicts an elevator-type movement for this protein though this prediction has not yet been experimentally tested[26].

Several shared structural features are immediately apparent upon looking at the structures of Glt_{Ph}, VcINDY and VcCNT. All three transporters have similar overall architecture, with a

scaffold domain wrapped around a transport domain, and all are oligomers (VcINDY is a dimer, Glt_{Ph} and VcCNT are trimers), possibly to aid in stabilization. In all three cases, the transport domain contains two re-entrant hairpin loops that dip into the membrane but do not cross it: the tips of these re-entrant loops coordinate substrates in all three transporters. Finally, all three folds contain a broken helix whose two segments are connected through an intramembrane loop (helices 5 and 10 in VcINDY, see Fig. 2a) that also contributes to the substrate-binding region.

Seemingly, a major mechanistic difference between Glt_{Ph} and VcINDY is that in Glt_{Ph} the reentrant hairpin loops act as inner and outer gates that cover the substrate binding site and regulate substrate binding/release. In both the inward-facing structure and the outward-facing model of VcINDY, the substrate is almost completely solvent exposed (Fig. 2), obviating the need for such gate movement. However, the electron density in the VcINDY crystal structure is ascribed to citrate, which is, in fact, a low affinity inhibitor[17]. Thus, our current analysis of the inhibitor-bound structure/model may miss some more subtle structural changes, for example, gate movement.

Recent reports provide evidence that several transporter families have essentially the same fold as VcINDY[22,36]. These transporters include the human Na^+ P_i transporter, NaPi-II[36]; and two recently structurally characterized representatives from the p-aminobenzoyl-glutamate transporter (AbgT) family, YdaH and MtrF[22,37,38]. The DASS family, to which VcINDY belongs, and the AbgT family, are both members of the Ion Transporter (IT) superfamily, strongly indicating that the elevator-type movement is a common mechanism for all IT superfamily members. Clearly, the mechanism underlying transport by the other IT superfamily members must be investigated, but the commonality of this architecture hints at widespread use of this mechanism.

Mammalian homologs of VcINDY are potential drug targets in the treatment of metabolic diseases, age-related diabetes and obesity[16,39]. VcINDY is ~30% identical and shares a number of functional characteristics, such as substrate specificity and coupling ion stoichiometry, with its mammalian homologs, in particular hNaDC3[17]. In addition, both VcINDY and hNaDC3 are allosterically inhibited by the anthranilic acid derivative, flufenamic acid, which is thought to interact at the interface between the scaffold and the transport domain[17,40,41]. These fundamental mechanistic similarities strongly suggest that the overall architecture and basic mechanism of transport are similar in all members of the DASS family. By extension, it would appear that the elevator-type motion is also an essential part of the transport cycle in the mammalian counterparts. Further work is required to explicitly demonstrate a shared conformational mechanism for this family of transporters.

Why would the elevator-type mechanism be favored over other transport mechanisms such as, say a “rocking bundle” mechanism? One apparently common characteristic of several potential elevator- type transporters is the tendency to couple substrate transport to multiple (≥3) coupling ions. At equilibrium, increasing the number of coupling ions (n) dramatically increases the capacity for substrate accumulation, with this increase changing as the nth power of the ion gradient. We speculate that an elevator mechanism might be a useful way to

insulate the transporter from back-leak of substrate or coupling ions since, in contrast with "rocking bundle" transporters, it can never contain a continuous return path.

Note added in proof: After this work was accepted, structures of a citrate:sodium symporter from *Salmonella enterica* (SeCitS) were reported, revealing an elevator-like conformational change involving a 16 Å translation and 31° rotation[42]. The fold of CitS differs from that of VcINDY in that the helical hairpin follows the unbroken helix in each repeat of CitS, rather than preceding it, as in VcINDY. However, the two structures share a common arrangement of scaffold and transport domains, providing additional support to the mechanism for VcINDY reported here.

Online Methods

Model building

A VcINDY outward-facing model was obtained by applying the repeat-swapped homology modeling technique following a recently updated protocol. The repeats in the VcINDY structure, PDB ID: 4F35, were defined as comprising residues 42–242 for repeat unit 1 (RU1) and 253–462 for repeat unit 2 (RU2). TM-align was used to structurally superimpose these repeats[43], yielding template modeling scores (TM-scores), which give a measure of structural similarity that is independent of segment length (values between 0 and 1; 1 being structurally identical). The obtained TM-scores support the RMSD data reported in Results; specifically, superimposing the entirety of each repeat gave a TM-score of 0.52, which increased to 0.78 and 0.83 when comparing only the transport and scaffold domain helices, respectively. The analysis of the symmetry axis of the repeats was performed using SymD[44]. . An initial sequence alignment of the template and the model sequences was compiled from the TM-align output. This initial alignment was refined by removing gaps within secondary structural elements (obtained from DSSP[45,46]) and by using conservation scores (obtained from the ConSurf server with default settings[47]) to position conserved residues so that they were preferentially oriented toward the inside of the protein. After each adjustment to the alignment, 200 iterations of restraint optimization were performed using MODELLER v9.13[48] to check whether the resultant models exhibited improvements in the MolPDF and ProQM[49] scores as well as Procheck analysis[50].

The refined, final alignment (Supplementary Fig. 1) was then used to generate a set of 2000 repeat-swapped 3D models of which the best model was selected as that which best met the following criteria: the lowest MolPDF score, the highest global ProQM score, and the most residues in favored regions of the Ramachandran plot. This model was then used to identify the scaffold and transport domains, which were assigned as residues 19–126 plus 253–356, and 127–242 plus 357–462, respectively. Final refinement of the model involved adding distance restraints between Cα atoms taken from the known structure in addition to those necessary to position the ions and bound ligand in the binding site. Distance restraints between Cα atoms were assigned according to the input crystal structure for all pairs of Cα atoms <60 Å apart within either the transport or scaffold domains in the template structure, PDB ID: 4F35. We note that these intradomain restraints did not alter the extent of the conformational movement, but maintained the internal arrangement of the two domains (Supplementary Figs. 2b and 9). Distance restraints were also applied in the substrate

binding sites: between the Na^+ ion and the O atoms in the backbone of S146, S150 and N199, the hydroxyl group of S146 and the amide group of N151; and between any non-hydrogen atoms of the substrate mimic (citrate) and the protein within 3.5Å in the template structure. All applied distance restraints were represented as Gaussians with a standard deviation of 0.1 Å. Using these restraints, a new set of 2000 models was generated using MODELLER, and again the final model was chosen using the criteria mentioned above.

The orientation of the VcINDY X-ray structure in the membrane was determined with the OPM server[51]. The orientation of the protomer model was defined after superposition of the scaffold domain onto that of the crystal structure. A dimeric model was constructed by superposing the same model onto both protomers in the crystal structure, and using MODELLER to locally refine residues in the interface, defined as any residues containing an atom within 5 Å of the other protomer in the model after superposition (residues 63 to 113 of TM3-TM4b and residues 286 to 339 of TM8-TM9b). The RMSD of the refined model compared to the initial model was 0.17 Å over all atoms. For the analysis of the transport- scaffold interface, we selected all residues with any atom within 5 Å of the other domain in either inward- or outward-facing conformation. In the case of Glt_{Ph} PDB entries 3KBC (inward-facing) and 1XFH (outward-facing) were used. All molecular figures and movies were generated using PyMOL v1.6 (Schrödinger, Ltd) unless stated otherwise. The final model is provided as Supplementary Data, and has been submitted to the Protein Model Database[52](https://bioinformatics.cineca.it/PMDB/) with identifier PM0080216.

Molecular biology and cysteine mutant design

All mutants were made using the Quikchange II site directed mutagenesis kit (Agilent Technologies) and were fully sequenced to ensure sequence fidelity. All cysteine mutants were generated in cysteine-free background where all three native cysteines in VcINDY were substituted for serine.

In total, we introduced 18 different combinations of double cysteine mutants into the interface between the transport and scaffold domains. However, most of these mutant combinations resulted in unstable protein that expressed poorly or aggregated (Supplementary Table 1). The majority of these cysteine substitutions were located towards the center of the transport domain in positions with low solvent accessibility. Only one of the “buried” interfacial pairs that we tested, T154C V272C, yielded stable protein and was used in further studies (Fig. 2b). The distance between the Cβ-Cβ atoms of T154 (from HP1) and V272 (from TM7) in the inward-facing structure (d_{ifs}) is 18.7 Å, whereas in the outward-facing model the distance (d_{ofm}) is 3.9 Å. We subsequently targeted regions at the periphery of the interface, in particular the symmetry related helices 4c and 7c. Solvent accessible loops were more tolerant to modification so we were able to introduce two cysteine pairs, A120C V165C in helix 4c/HP1 (d_{ifs} = 11.7 Å; d_{ofm} = 4.7 Å), and A346C V364C in helix 9c/HP2 (d_{ifs} = 16 Å; d_{ofm} = 5.6 Å), with no apparent reduction in protein stability (Fig. 2b). For the inward-facing control mutant, L60C S381C, d_{ifs} = 6.9 Å; d_{ofm} = 20.6 Å,

Protein expression and purification

VcINDY and its variants were expressed and purified as detailed previously. VcINDY was expressed in Escherichia coli BL21-AI cells (Life Technologies) from a modified pET vector in frame with an N-terminal decahistidine tag[53]. Cells were grown in LB supplemented with 30 ug/ml kanamycin at 37°C until they reached an A_{600} of 0.8, at which point they were rapidly cooled to 19°C in an ice bath. Expression was induced by addition of IPTG and L-arabinose to final concentrations of 10 μM and 6.6 mM, respectively. Cells were incubated overnight at 19°C. Cells were harvested and resuspended in Lysis Buffer (50 mM Tris, pH 8, 400 mM NaCl and 20% glycerol), and lysed using a homogenizer (Emulsiflex-C3, Avestin). The membrane fraction was isolated by ultracentrifugation, resuspended in Purification Buffer (50 mM Tris, pH 8, 200 mM NaCl and 10% glycerol), and solubilized by addition of n-dodecyl-β-D- maltoside (DDM, Anatrace) to a final concentration of 20 mM. Residual insoluble material was removed by ultracentrifugation and the soluble fraction was incubated with Talon metal affinity resin (Takara Bio Inc.) overnight at 4°C. Resin was washed by consecutive additions of 20 column volumes-worth of 10 mM and 20 mM imidazole-containing Purification Buffer supplemented with 2 mM DDM. Bound protein was eluted whilst simultaneously cleaving the affinity tag by incubating the resin with Purification Buffer supplemented with 2 mM DDM and 10 μg/ml trypsin at 4°C for 1 hour. The flow through from the column was collected, concentrated and further purified using a Superdex 200 size exclusion chromatography (SEC) column (GE Healthcare) equilibrated with SEC buffer (25 mM Tris pH, 100 mM NaCl, 5% glycerol and 3 % *n*-decyl-β-D-maltoside (DM)). For the dimer interface mutants, protein was eluted from the Talon resin by addition of Purification Buffer supplemented with 300 mM imidazole. The affinity tag was maintained for identification of the protein using Western blotting. The dimer interface mutants were then desalted into SEC buffer using Zeba Spin desalting columns (Life Technologies). Purified protein was concentrated, snap frozen and stored at −80°C. All proteins were purified using buffers containing either 0.5 mM tris(2-carboxyethyl)phosphine (TCEP) or 1 mM dithiothreitol (DTT) to keep the cysteines reduced. For detection of His-tagged protein, Western blotting was used with anti-Penta-His antibody (Qiagen).

Reconstitution

The functional reconstitution of protein into liposomes was performed as detailed previously[54]. 25–100 μg of purified protein was diluted to 2 ml in SEC buffer (with 1 mM DTT, if required) and mixed with 400 μl 20 mg/ml lipids, which consisted of a 3:1 mixture of E. coli polar lipids and POPC (Avanti Polar Lipids, Inc). The protein/lipid mixture was incubated on ice for 10 min and then rapidly diluted into 65 ml Inside Solution containing 20 mM Tris/HEPES, pH 7.5, 1 mM NaCl, 199 mM KCl and 0.5 mM TCEP/1 mM DTT, where required. Proteoliposomes were collected by ultracentrifugation and resuspended in Inside Solution to a concentration of 8 mg/ml lipid. Proteoliposomes were freeze-thawed 3 times and stored at −80°C or used immediately. After this point, the internal solution was modified by collecting the proteoliposomes by centrifugation, resuspending them in the desired solution, freeze-thawing 3 times and extruding.

In vitro transport assays

Proteoliposomes were prepared for transport assays by extruding them through a 400 nm filter 11 times and concentrating them to 80 mg/ml lipid using ultracentrifugation. The transport assays were started by adding the proteoliposomes to Reaction Buffer (20 mM Tris/HEPES, pH 7.5, 100 mM NaCl, 100 mM KCl, 1 μM valinomycin, 1 μM [^{3}H]-succinic acid (American Radiolabeled Chemicals). At the indicated times, samples were taken and the reaction was terminated by adding the sample to ice cold Quench buffer (20 mM Tris/HEPES, pH 7.5, 200 mM ChCl) and rapidly filtering the sample through a 200 nm nitrocellulose filter (Millipore). The filter was washed with 3 ml Quench buffer, the filters were dissolved in FilterCount liquid scintillation cocktail (PerkinElmer) and the [^{3}H]-succinic acid internalized by the proteoliposomes was counted using a Trilux beta counter (PerkinElmer).

Protein crosslinking and PEGylation assay

To induce disulfide bond formation in detergent solubilized protein (as in the band-shift assay), the proteins were exchanged into Conjugation Buffer (50 mM Tris, pH 7, 100 mM NaCl, 5 % glycerol, and 3% (w/v) DM) using Zeba Spin Desalting Columns (ThermoFisher Scientific) to remove the reducing agent and then incubated with 5-fold molar excess of $HgCl_2$ or freshly prepared solution of copper phenanthroline (CuPhen). A 2:1 ratio of CuPhen was prepared by mixing solutions of 500 mM 1,10-phenanthroline and 250 mM $CuSO_4$. The final CuPhen concentration ranged from 10 to 500 μM depending on the particular cysteine mutant. Regardless of which crosslinking reagent was being used, the crosslinking reaction was incubated at room temperature for 45 min. Control samples were treated identically except were incubated in the presence of 0.5 mM TCEP or 1 mM DTT. Following this incubation, the crosslinker was removed by exchanging the protein into Conjugation Buffer containing no crosslinking agent. To PEGylate any free cysteines, the protein samples were then incubated for 3 hours at room temperature in the presence of 0.5 % (w/v) SDS and 2 mM mPEG5K. Proteins were separated on non-reducing 12% polyacrylamide gels, which were stained with Coomassie dye to visualize the protein.

Crosslinking the proteins already incorporated into liposomes was achieved by adding 50 μM $HgCl_2$ to the liposome suspension. To facilitate internalization of the $HgCl_2$, the treated proteoliposomes underwent three freeze-thaw cycles and were extruded through a filter with a 0.4 μm pore size. Following freeze-thaw treatment and extrusion the liposomes were incubated for 30 min at room temperature. $HgCl_2$ was removed by exchanging the solutions on both sides of the membrane for Inside Buffer. This exchange was performed by pelleting the proteoliposomes by ultracentrifugation, then resuspension in the desired buffer. At this stage, 1 mM DTT was added, where appropriate. Solutions were equilibrated across the membrane, again by three freeze-thaw cycles and extrusion. Original images of gels and blots used in this study can be found in Supplementary Data Set 1

Unexpectedly, Cysless VcINDY showed less activity in the presence of Hg^{2+} than under reducing conditions (Fig. 5), however this effect actually reflects an enhancement of activity due to the reducing agent, DTT (Supplementary Fig. 6c). Indeed, the presence of increasing

amounts of $HgCl_2$ if anything actually increased the Cysless protein's transport activity (Supplementary Fig. 6d).

Protein Digestion and Mass Spectrometry

Protein samples, at 10 μM, in 50 mM Tris pH 7, 150 mM NaCl, 5% glycerol, 0.1% DM were either reduced with 1 mM DTT ('R') or treated with 100 μM or 500 μM CuPhen to induce disulfide formation ('X') followed by desalting to remove the reagent. ~5 μg of protein was alkylated by incubation with 10 mM N-ethylmaleimide (NEM, Sigma) for 20 min at room temperature. A120C/V165C was digested with 500 ng trypsin for 8 hr at 37°C and further digested with 300 ng chymotrypsin (Roche, Indianapolis, IN) for 8 hr at 25°C; T154C V272C was digested with 600 ng chymotrypsin at 25°C overnight. The digests were cleaned with an HLB μElution plate (Waters, Milford, MA). The LC/MS/MS experiments were performed on an Orbitrap Elite mass spectrometer (Thermo Scientific) connected to a 3000 RSLC nano HPLC system with an RS auto-sampler (Thermo-Dionex) via an Easy-Spray ion source (Thermo Scientific). Approximately 1 μg of digested protein was injected onto an ES802 Easy-Spray column (25 cm × 75 μm ID, PepMap RSLC C18 2 μm; Thermo Scientific) and then separated at a flow rate of 300 nl/min with a 38 min linear gradient of 2–30% mobile phase B (mobile phase A: 2% acetonitrile, 0.1% formic acid; mobile phase B: 98% acetonitrile, 0.1% formic acid).

The Orbitrap Elite was operated in a decision tree mode. The precursor ion scan was performed in the Orbitrap with a resolution of 60K at m/z 400. The m/z range for survey scans was 300–1600. The fragment ion scan was performed in the linear ion trap. The minimum signal threshold for MS/MS scan was set to 3×10^4, and up to 10 MS/MS scans were performed after each MS scan. A 9 sec dynamic exclusion window was selected with early expiration enabled.

Peptide Identification

Mascot Distiller (version 2.5.1.0) was used to convert the Xcalibur Raw data to peak list file in mgf format. Mascot Daemon 2.4.0 was used to submit the MGF files to Mascot Server 2.4 for the database search. Data were searched against a house-built database that contains the sequences of NCBI human database and the sequences of A120C V165C, T154C V272C, and A346C V364C. The following parameters were included in the search: Peptide tolerance, ± 10 ppm; MS/MS tolerance, 0.2 Da; Instrument type, CID+ETD; Enzyme, None; Missed cleavage, 0; Variable modification, Oxidation (M) and NEM (C). Once a peptide (Px) containing a Cys residue was detected, a 2nd database search was performed assuming Px-2H (the mass of Px minus 2 hydrogen atoms) as a potential modification. Once a plausible cross-linked candidate was found in the 2nd search, the MS/MS spectrum of that candidate was manually checked. A potentially cross-linked candidate was considered real if the following conditions were satisfied: 1) Major peaks of the MS/MS spectrum of the cross-linked candidate could be assigned manually; 2) The candidate was only detected in the X samples, not in the corresponding R samples.

Supplementary Material

Refer to Web version on PubMed Central for supplementary material.

Acknowledgments

We thank A. Banerjee for helpful discussions and M. Maduke, J. Faraldo-Gómez, G. Rudnick, and M. Mayer for critical reviews of the manuscript. AVJ is recipient of the L'Oreal Chile-UNESCO Women in Science Fellowship and the L'Oreal-UNESCO Rising Talent Award. This work was supported by the Division of Intramural Research of the US National Institutes of Health, National Institute of Neurological Disorders and Stroke.

References

1. Jardetzky O. Simple allosteric model for membrane pumps. Nature. 1966; 211:969–70. [PubMed: 5968307]
2. Mitchell P. A general theory of membrane transport from studies of bacteria. Nature. 1957; 180:134–6. [PubMed: 13451664]
3. Boudker O, Ryan RM, Yernool D, Shimamoto K, Gouaux E. Coupling substrate and ion binding to extracellular gate of a sodium-dependent aspartate transporter. Nature. 2007; 445:387–93. [PubMed: 17230192]
4. Krishnamurthy H, Piscitelli CL, Gouaux E. Unlocking the molecular secrets of sodium-coupled transporters. Nature. 2009; 459:347–55. [PubMed: 19458710]
5. Yamashita A, Singh SK, Kawate T, Jin Y, Gouaux E. Crystal structure of a bacterial homologue of Na+/Cl−-dependent neurotransmitter transporters. Nature. 2005; 437:215–23. [PubMed: 16041361]
6. Reddy VS, Shlykov MA, Castillo R, Sun EI, Saier MH Jr. The major facilitator superfamily (MFS) revisited. FEBS J. 2012; 279:2022–35. [PubMed: 22458847]
7. Vastermark A, Saier MH Jr. Evolutionary relationship between 5+5 and 7+7 inverted repeat folds within the amino acid-polyamine-organocation superfamily. Proteins. 2014; 82:336–46. [PubMed: 24038584]
8. Fowler PW, et al. Gating topology of the proton-coupled oligopeptide symporters. Structure. 2015; 23:290–301. [PubMed: 25651061]
9. Kazmier K, Sharma S, Islam SM, Roux B, McHaourab HS. Conformational cycle and ion-coupling mechanism of the Na+/hydantoin transporter Mhp1. Proc Natl Acad Sci U S A. 2014; 111:14752–7. [PubMed: 25267652]
10. Kazmier K, et al. Conformational dynamics of ligand-dependent alternating access in LeuT. Nat Struct Mol Biol. 2014; 21:472–9. [PubMed: 24747939]
11. Krishnamurthy H, Gouaux E. X-ray structures of LeuT in substrate-free outward-open and apo inward-open states. Nature. 2012; 481:469–74. [PubMed: 22230955]
12. Shimamura T, et al. Molecular basis of alternating access membrane transport by the sodium-hydantoin transporter Mhp1. Science. 2010; 328:470–3. [PubMed: 20413494]
13. Crisman TJ, Qu S, Kanner BI, Forrest LR. Inward-facing conformation of glutamate transporters as revealed by their inverted-topology structural repeats. Proc Natl Acad Sci U S A. 2009; 106:20752–7. [PubMed: 19926849]
14. Reyes N, Ginter C, Boudker O. Transport mechanism of a bacterial homologue of glutamate transporters. Nature. 2009; 462:880–5. [PubMed: 19924125]
15. Lee C, et al. A two-domain elevator mechanism for sodium/proton antiport. Nature. 2013; 501:573–7. [PubMed: 23995679]
16. Bergeron MJ, Clemencon B, Hediger MA, Markovich D. SLC13 family of Na(+)-coupled di- and tri-carboxylate/sulfate transporters. Mol Aspects Med. 2013; 34:299–312. [PubMed: 23506872]
17. Mulligan C, Fitzgerald GA, Wang DN, Mindell JA. Functional characterization of a Na+-dependent dicarboxylate transporter from Vibrio cholerae. J Gen Physiol. 2014; 143:745–59. [PubMed: 24821967]

18. Saier MH Jr, Tran CV, Barabote RD. TCDB: the Transporter Classification Database for membrane transport protein analyses and information. Nucleic Acids Res. 2006; 34:D181–6. [PubMed: 16381841]
19. Mancusso R, Gregorio GG, Liu Q, Wang DN. Structure and mechanism of a bacterial sodium-dependent dicarboxylate transporter. Nature. 2012; 491:622–6. [PubMed: 23086149]
20. Chen JS, et al. Phylogenetic characterization of transport protein superfamilies: superiority of SuperfamilyTree programs over those based on multiple alignments. J Mol Microbiol Biotechnol. 2011; 21:83–96. [PubMed: 22286036]
21. Prakash S, Cooper G, Singhi S, Saier MH Jr. The ion transporter superfamily. Biochim Biophys Acta. 2003; 1618:79–92. [PubMed: 14643936]
22. Vergara-Jaque A, Fenollar-Ferrer C, Mulligan C, Mindell JA, Forrest LR. Family resemblances: A common fold for some dimeric ion-coupled secondary transporters. J Gen Physiol. 2015; 146:423–34. [PubMed: 26503722]
23. Forrest LR, et al. Mechanism for alternating access in neurotransmitter transporters. Proc Natl Acad Sci U S A. 2008; 105:10338–43. [PubMed: 18647834]
24. Radestock S, Forrest LR. The alternating-access mechanism of MFS transporters arises from inverted-topology repeats. J Mol Biol. 2011; 407:698–715. [PubMed: 21315728]
25. Schushan M, et al. A model-structure of a periplasm-facing state of the NhaA antiporter suggests the molecular underpinnings of pH-induced conformational changes. J Biol Chem. 2012; 287:18249–61. [PubMed: 22431724]
26. Vergara-Jaque A, Fenollar-Ferrer C, Kaufmann D, Forrest LR. Repeat-swap homology modeling of secondary active transporters: updated protocol and prediction of elevator-type mechanisms. Front Pharmacol. 2015; 6:183. [PubMed: 26388773]
27. Basilio D, Noack K, Picollo A, Accardi A. Conformational changes required for H(+)/Cl(−) exchange mediated by a CLC transporter. Nat Struct Mol Biol. 2014; 21:456–63. [PubMed: 24747941]
28. Groeneveld M, Slotboom DJ. Rigidity of the subunit interfaces of the trimeric glutamate transporter GltT during translocation. J Mol Biol. 2007; 372:565–70. [PubMed: 17673229]
29. Forrest LR, Tang CL, Honig B. On the accuracy of homology modeling and sequence alignment methods applied to membrane proteins. Biophys J. 2006; 91:508–17. [PubMed: 16648166]
30. Olivella M, Gonzalez A, Pardo L, Deupi X. Relation between sequence and structure in membrane proteins. Bioinformatics. 2013; 29:1589–92. [PubMed: 23677941]
31. Yernool D, Boudker O, Jin Y, Gouaux E. Structure of a glutamate transporter homologue from Pyrococcus horikoshii. Nature. 2004; 431:811–8. [PubMed: 15483603]
32. Paulino C, Wohlert D, Kapotova E, Yildiz O, Kuhlbrandt W. Structure and transport mechanism of the sodium/proton antiporter MjNhaP1. Elife. 2014; 3:e03583. [PubMed: 25426803]
33. Wohlert D, Kuhlbrandt W, Yildiz O. Structure and substrate ion binding in the sodium/proton antiporter PaNhaP. Elife. 2014; 3:e03579. [PubMed: 25426802]
34. Johnson ZL, Cheong CG, Lee SY. Crystal structure of a concentrative nucleoside transporter from Vibrio cholerae at 2.4 A. Nature. 2012; 483:489–93. [PubMed: 22407322]
35. Johnson ZL, et al. Structural basis of nucleoside and nucleoside drug selectivity by concentrative nucleoside transporters. Elife. 2014; 3:e03604. [PubMed: 25082345]
36. Fenollar-Ferrer C, et al. Structural fold and binding sites of the human Na(+)-phosphate cotransporter NaPi-II. Biophys J. 2014; 106:1268–79. [PubMed: 24655502]
37. Bolla JR, et al. Crystal structure of the Alcanivorax borkumensis YdaH transporter reveals an unusual topology. Nat Commun. 2015; 6:6874. [PubMed: 25892120]
38. Su CC, et al. Structure and function of Neisseria gonorrhoeae MtrF illuminates a class of antimetabolite efflux pumps. Cell Rep. 2015; 11:61–70. [PubMed: 25818299]
39. Colas C, Pajor AM, Schlessinger A. Structure based identification of inhibitors for the SLC13 family of Na+/dicarboxylate cotransporters. Biochemistry. 2015
40. Burckhardt BC, Lorenz J, Burckhardt G, Steffgen J. Interactions of benzylpenicillin and non-steroidal anti-inflammatory drugs with the sodium-dependent dicarboxylate transporter NaDC-3. Cell Physiol Biochem. 2004; 14:415–24. [PubMed: 15319545]

41. Pajor AM, Sun NN. Nonsteroidal anti-inflammatory drugs and other anthranilic acids inhibit the Na(+)/dicarboxylate symporter from Staphylococcus aureus. Biochemistry. 2013; 52:2924–32. [PubMed: 23566164]
42. Wohlert D, Grotzinger MJ, Kuhlbrandt W, Yildiz O. Mechanism of Na(+)-dependent citrate transport from the structure of an asymmetrical CitS dimer. Elife. 2015; 4
43. Zhang Y, Skolnick J. TM-align: a protein structure alignment algorithm based on the TM-score. Nucleic Acids Res. 2005; 33:2302–9. [PubMed: 15849316]
44. Tai CH, Paul R, Dukka KC, Shilling JD, Lee B. SymD webserver: a platform for detecting internally symmetric protein structures. Nucleic Acids Res. 2014; 42:W296–300. [PubMed: 24799435]
45. Edgar RC. Quality measures for protein alignment benchmarks. Nucleic Acids Res. 2010; 38:2145–53. [PubMed: 20047958]
46. Kabsch W, Sander C. Dictionary of protein secondary structure: pattern recognition of hydrogen-bonded and geometrical features. Biopolymers. 1983; 22:2577–637. [PubMed: 6667333]
47. Ashkenazy H, Erez E, Martz E, Pupko T, Ben-Tal N. ConSurf 2010: calculating evolutionary conservation in sequence and structure of proteins and nucleic acids. Nucleic Acids Res. 2010; 38:W529–33. [PubMed: 20478830]
48. Sali A, Blundell TL. Comparative protein modelling by satisfaction of spatial restraints. J Mol Biol. 1993; 234:779–815. [PubMed: 8254673]
49. Ray A, Lindahl E, Wallner B. Model quality assessment for membrane proteins. Bioinformatics. 2010; 26:3067–74. [PubMed: 20947525]
50. Laskowski RA, Macarthur MW, Moss DS, Thornton JM. Procheck - a Program to Check the Stereochemical Quality of Protein Structures. Journal of Applied Crystallography. 1993; 26:283–291.
51. Lomize MA, Lomize AL, Pogozheva ID, Mosberg HI. OPM: orientations of proteins in membranes database. Bioinformatics. 2006; 22:623–5. [PubMed: 16397007]
52. Castrignano T, De Meo PD, Cozzetto D, Talamo IG, Tramontano A. The PMDB Protein Model Database. Nucleic Acids Res. 2006; 34:D306–9. [PubMed: 16381873]
53. Love J, et al. The New York Consortium on Membrane Protein Structure (NYCOMPS): a high-throughput platform for structural genomics of integral membrane proteins. J Struct Funct Genomics. 2010; 11:191–9. [PubMed: 20690043]
54. Mulligan C, et al. The substrate-binding protein imposes directionality on an electrochemical sodium gradient-driven TRAP transporter. Proc Natl Acad Sci U S A. 2009; 106:1778–83. [PubMed: 19179287]

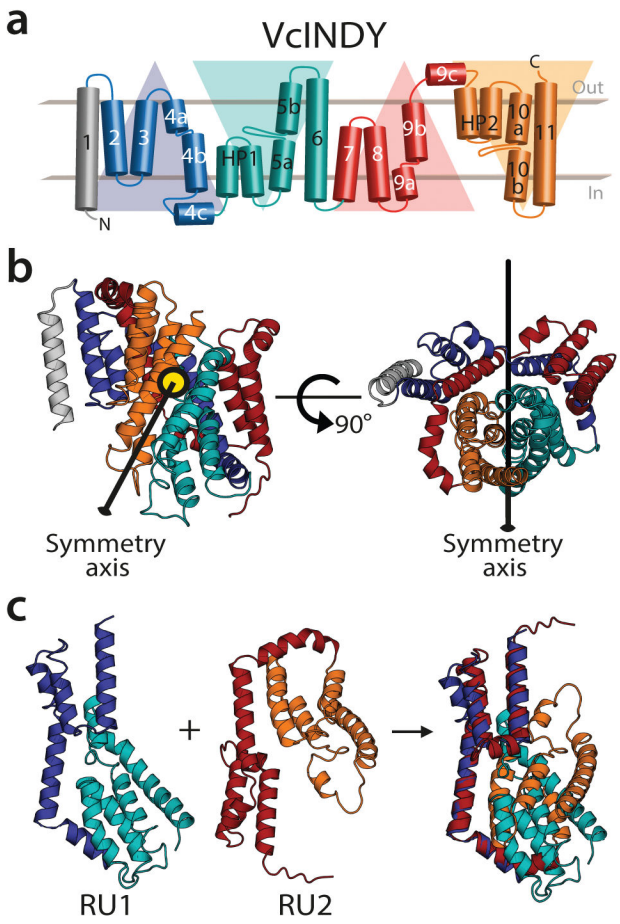

Figure 1. Repeat-swap modeling of VcINDY

(a) Schematic representation of the topology of VcINDY colored according to the structural repeats. The blue and cyan helices comprise repeat unit 1 (RU1), while repeat unit 2 (RU2) is composed of the red and orange helices. **(b)** Cartoon representation of the X-ray crystal structure of a VcINDY protomer showing that RU1 is related to RU2 by two-fold pseudo-symmetry, with the symmetry axis parallel to the membrane. The black arrow represents the symmetry axis within the structure of the VcINDY protomer, viewed from within the plane of the membrane (*left*) and from the extracellular side of the protein (*right*). **(c)** A cartoon representation showing a structural alignment, built with TM-Align, of the repeats with the helices colored according to the topology in **(a)**. The initial sequence alignment used to build a swapped-repeat model was generated based on this structural alignment.

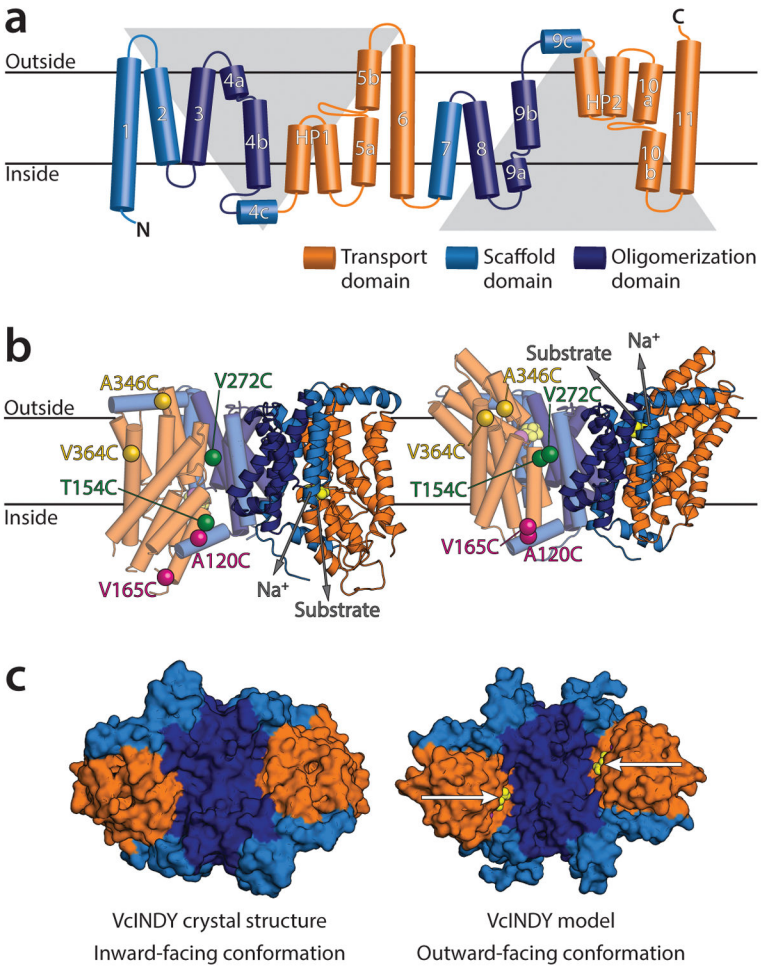

Figure 2. Identification of VcINDY transporter domains

(a) Topology diagram of a VcINDY protomer colored according to the helices forming the scaffold (*light blue*), oligomerization (*dark blue*) and transport (*orange*) domains. Gray triangles indicate RU1 (down triangle) and RU2 (up triangle), respectively. **(b)** Cartoon representation of the dimeric VcINDY X-ray crystal structure in an inward-facing conformation (*left*) and the model in an outward-facing conformation (*right*) viewed from the membrane plane. Substrate and Na^+ are shown asspheres, with their pathways indicated by gray arrows. Cα-atoms of the residues studied by crosslinking are shown as spheres colored in pairs (*left-hand side protomers*). **(c)** Surface representation of the VcINDY X-ray crystal structure (*left*) and model (*right*) viewed from the extracellular side. The substrate (*yellow spheres*, indicated by arrows) is visible from the extracellular side in the model (*right*), but not in the inward-facing crystal structure (*left*).

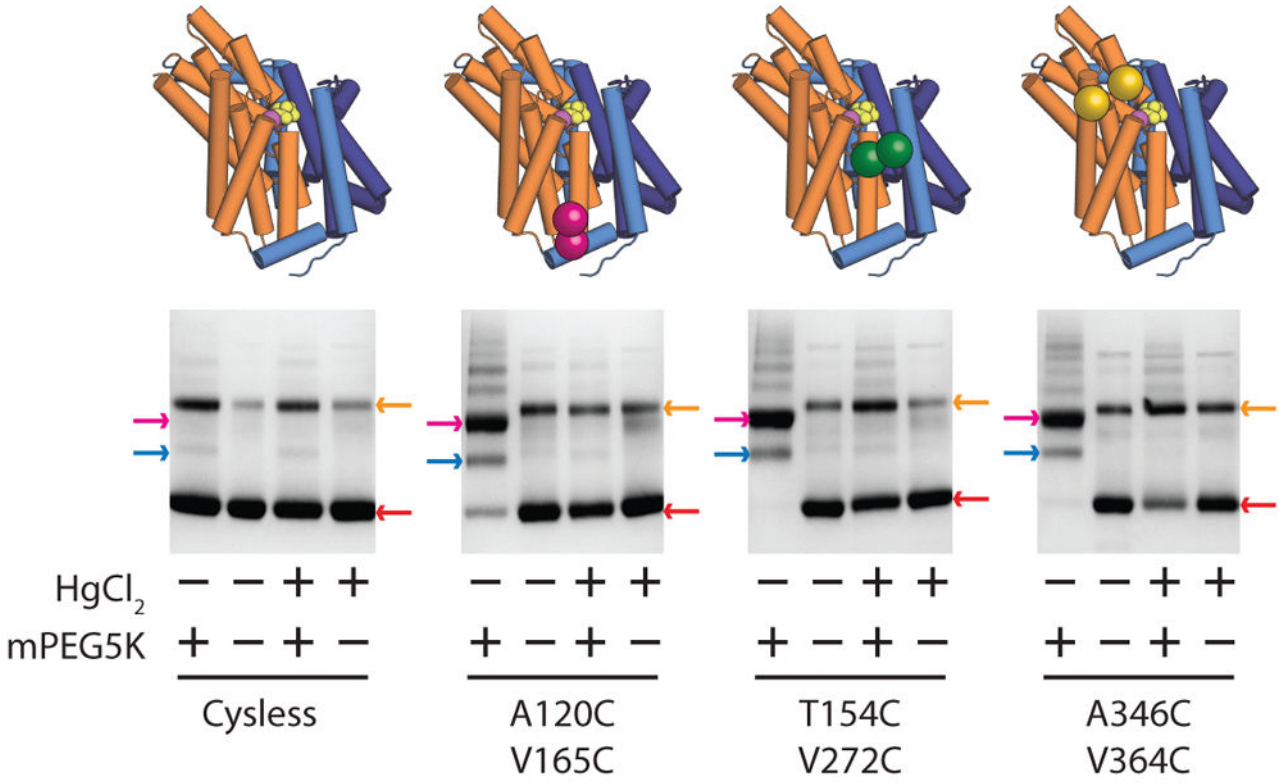

Figure 3. Chemical crosslinking of outward-stabilizing cysteine pairs

SDS-PAGE band-shift assay showing the number of free cysteines present in Cysless and the three double cysteine mutants; A120C V165C, T154C V272C, and A346C V364C, with (+) and without (−)prior treatment with $HgCl_2$. Relative positions of the cysteine pairs are shown in the cartoon representation of a VcINDY protomer (*top*). The following protein species seen in the gels are indicated by colored arrows; unmodified VcINDY (*red arrow*), dimeric VcINDY (*orange arrow*), singly PEGylated VcINDY (*blue arrow*), and doubly PEGylated VcINDY (*magenta arrow*). Non-reducing SDS-PAGE gels were used and protein was visualized using Coomassie dye. The assay was performed on at least two separate occasions with the same outcome.

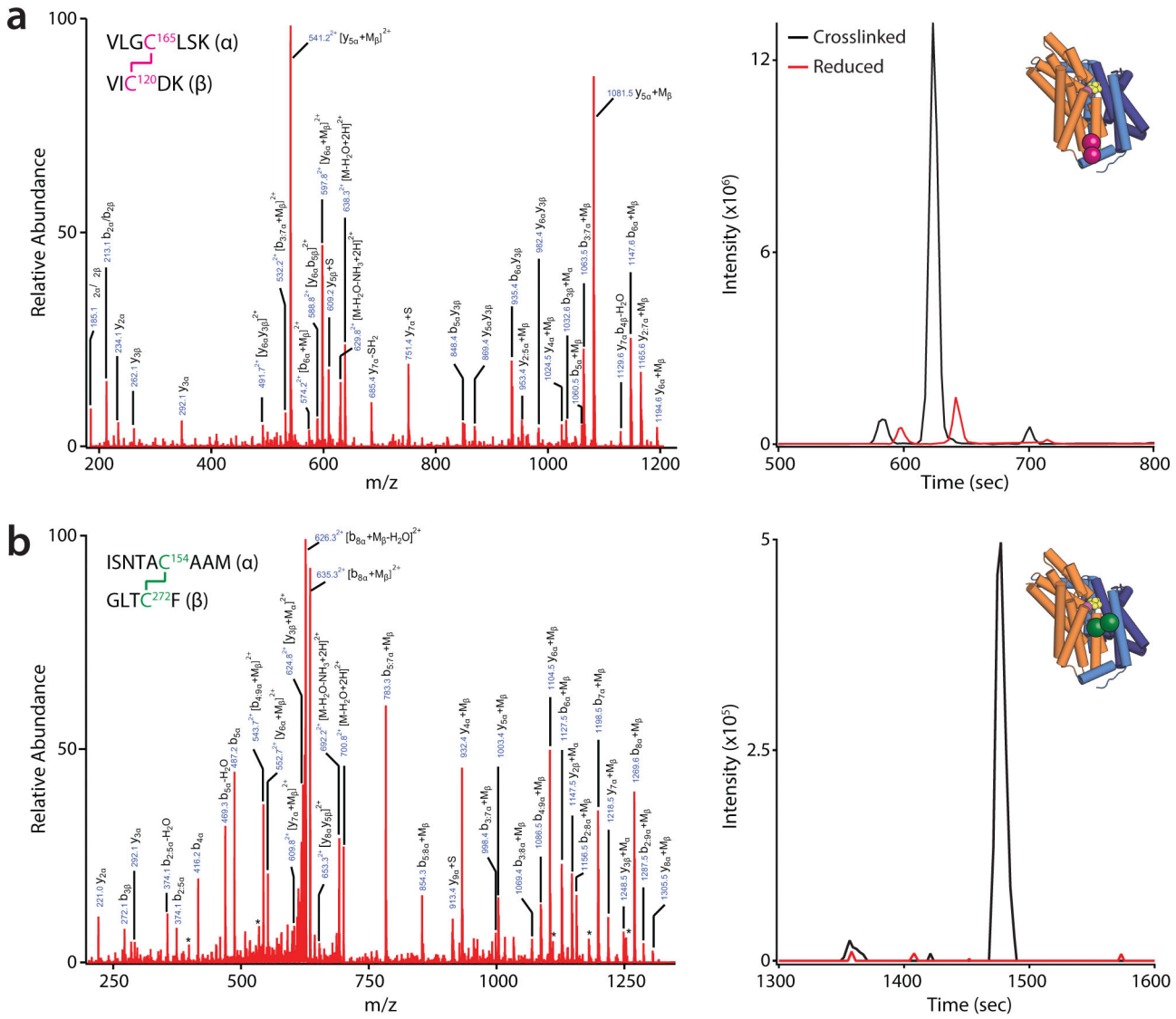

Figure 4. Mass spectrometric identification of crosslinked peptides

Representative LC-MS/MS spectra of disulfide-linked peptides detected from the digests of CuPhen-treated A120C V165C **(a)** and T154C V272C **(b)**. Collision-induced dissociation (CID) spectrum of the disulfide linked peptide(inset) from the proteolytic digests (*left*), and the associated extracted ion chromatogram (XIC, *right*) for protein treated with crosslinking reagent (*black line*) or maintained in reducing conditions (*red line*). This experiment was repeated twice with separately prepared and treated protein. The annotation "i:j represents fragments from internal cleavage. For example $y_{2:5}$ represents the peptide fragment from the 2nd to 5th residue; "*" represents fragments with a neutral loss of water.

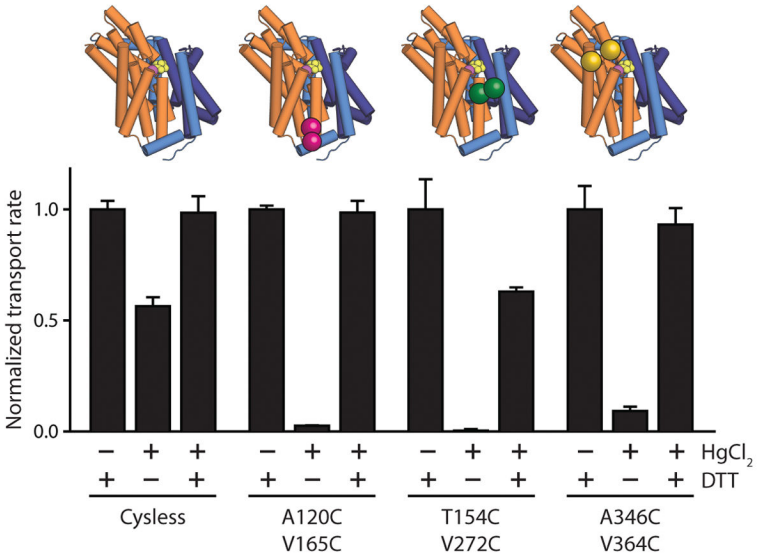

Figure 5. Stabilizing VcINDY in the outward-facing state abolishes transport

Normalized initial rates of [^{3}H]-succinate transport in the presence of proteoliposomes containing Cysless and the three double cysteine mutants compatible with the outward-facing state after treatment with(+) and without (−) $HgCl_2$ and DTT. Relative positions of cysteine pairs are shown as in Fig. 3. Results from triplicate datasets are shown and error bars represent S.E.M. This experiment was repeated twice with fresh preparations of proteoliposomes.

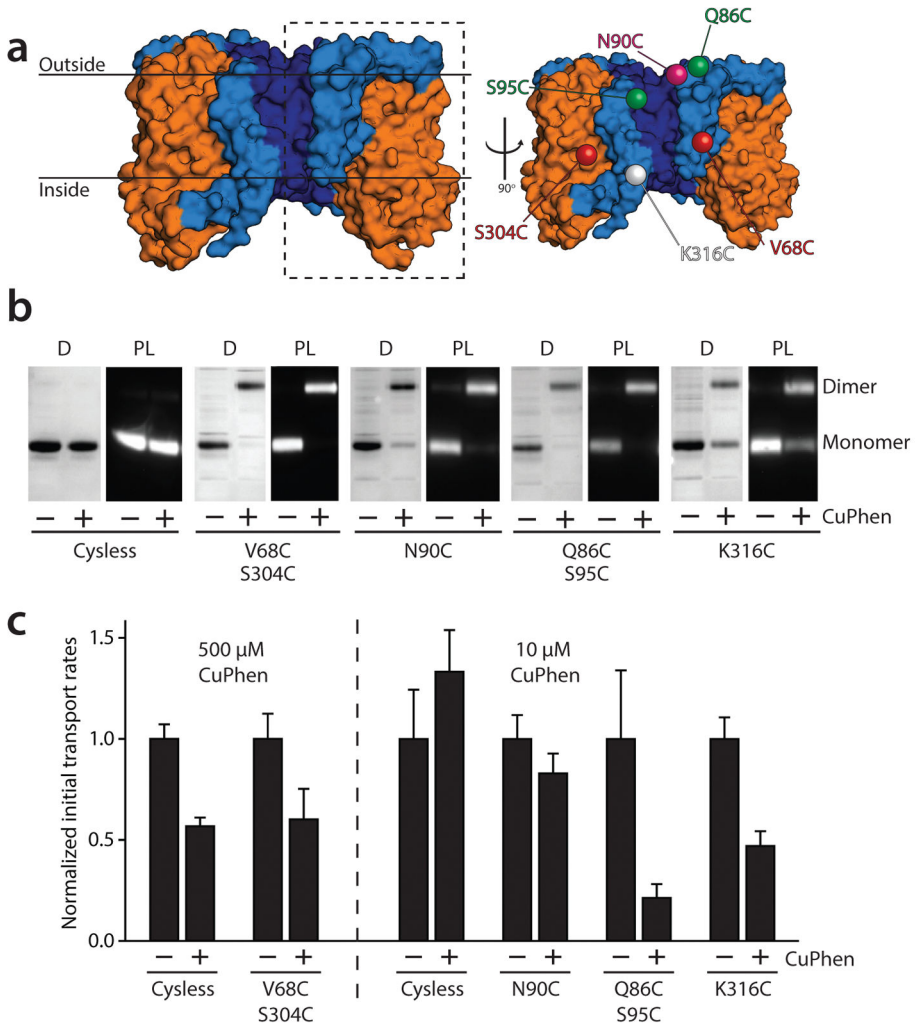

Figure 6. Constraining the dimer interface has minimal effects on transport

(a) Surface representation of a VcINDY dimer viewed from the plane of the membrane (*left*) and a VcINDY protomer viewed from the dimer interface (*right*), if the VcINDY dimer is opened like a book. Cylinders represent the interfacial α-helices that make the intra-protomer contacts across the dimer interface. The colored spheres represent the positions of cysteine residues introduced to staple the VcINDY protomers together. **(b)** Coomassie-stained SDS-PAGE gels of purified cysteine mutants in detergent solution ('D')and His-tag Western blot analysis of VcINDY-containing proteoliposomes ('PL') with (+) and without (−)treatment with CuPhen. In the absence of CuPhen treatment (−), disulfides were prevented by addition of 1 mM DTT. The positions of monomeric and dimeric VcINDY are indicated. **(c)** Normalized initial transport rates of Cysless and indicated cysteine mutants with (+) and without (−) treatment with CuPhen (concentration of CuPhen used is indicated in the figure). Results are from at least triplicate datasets and error bars represent S.E.M. Western blots were performed three separate times and transport assays were repeated at least twice with the same outcome.

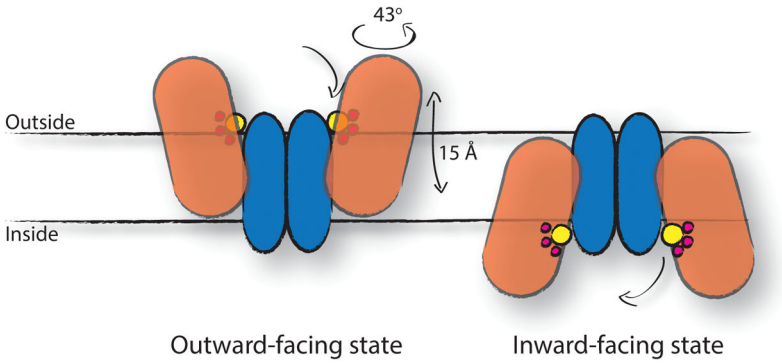

Figure 7. Proposed elevator-type transport mechanism in the VcINDY dimer

Cartoon representation of the transport mechanism inferred from the inward-facing crystal structure and outward-facing model of VcINDY. Blue shapes represent the scaffold and oligomerization domains and the orange shape is the transport domain. Substrates are represented by yellow spheres (succinate) and pink spheres (Na^+ ions). In our scheme, the substrates bind the outward-facing state of VcINDY (*left*, model) at which point the transport domain undergoes a ~15 Å translocation and ~43° rotation into the inward-facing state (*right*, crystal structure), where substrate can be released into the cytoplasm. Empty transporter must then recycle back to the outward-facing state to restart the cycle.